LA-UR-87-2636

CONF 8705168--3

Los Alamos National Laboratory is operated by the University of California for the United States Department of Energy under contract W-7405-ENG-36

LA-UR--87-2636

DE87 014736

TITLE EFFECTS OF IMPURITIES ON DOMAIN GROWTH

AUTHOR(S): D. J. Srolovitz
G. S. Grest
G. N. Hassold
R. Eykholt

SUBMITTED TO The Proceedings of Workshop "Competing Interactions and Microstructures: Statics and Dynamics," held in Los Alamos, May 5-8, 1987.

DISCLAIMER

Los Alamos National Laboratory
Los Alamos, New Mexico 87545

Effects of Impurities on Domain Growth

D. J. Srolovitz[∇,*], G. S. Grest[°], G. N. Hassold[*], and R. Eykholt[∇,#]

[∇]Los Alamos National Laboratory, Los Alamos, NM 87545
[*]Department of Materials Science and Engineering, University of Michigan, Ann Arbor, MI 48109
[°]Exxon Research and Engineering Co., Annandale, NJ 08801
[#]Department of Physics, Colorado State University, Fort Collins, CO 80523

1. Introduction

The kinetics of domain growth in simple spin models quenched from a high temperature ($T \gg T_c$) to a low temperature ($T < T_c$) have received a great deal of attention in the last 10 years. These spin systems provide a simple model for ordering processes in real materials (e.g., grain growth [1,2], spinodal decomposition [3], etc.). Such studies generally show that the correlation length in the system grows with time as t^n, where n is the temporal growth exponent. In cases with nonconservative dynamics, n is generally found to be 1/2. Occasional difficulties in obtaining this value (and the corresponding value of 1/3 for conservative systems) in Monte Carlo simulations are often attributable to finite system sizes (i.e., correlation length not sufficiently larger than lattice size). In many experimental systems, however, a growth exponent less than expected is observed [4]. Frequently, these low exponents are attributable to impurities in the experimental system. These impurities can take the form of second phase particles, atomic impurities, or lattice defects. At sufficiently low temperatures, these impurities are usually immobile and can be viewed as static or quenched with respect to the motion of domain wa ls. On the other hand, at sufficiently high temperatures where the impurity mobility is significant, the impurities can diffuse along with the moving domain walls. In either case, the impurities impede domain wall motion, resulting in slower growth kinetics.

In the present report, we consider the effects of both static and diffusing impurities on domain growth kinetics. In particular, we employ Monte Carlo simulations for nonconservative (Glauber) dynamics to examine the effects of quenched impurities on domain growth in the Potts model with varying degeneracy Q ($2 \le Q \le 48$) [5,6]. The effects of diffusing impurities are examined within the framework of the Ising model (i.e., Potts model with Q=2) as a function of impurity diffusivity [7]. Finally, a theoretical analysis of the diffusing-impurity results is presented [8]. Due to the limited space available, however, this paper presents only a review of our recent work, to which the interested reader is referred for more details [5-8].

2. Simulation Procedure

The Hamiltonian describing the Q-component ferromagnetic Potts model is written as

$$H = -J \sum_{NN} \delta_{S_i S_j} \qquad (1)$$

where S_i is the state of the spin on site i ($1 \le S_i \le Q$), δ_{AB} is the Kronecker δ function, and J is a positive constant. The summation in Eq. (1) is taken over all nearest neighbor (NN) spins on a two dimensional lattice. Since, in the present simulation, the order parameter is not conserved, spin-flip (Glauber) dynamics are employed. The Monte Carlo procedure employed was made more efficient by adoption of the technique known as the "n-fold way" [9]. In order to

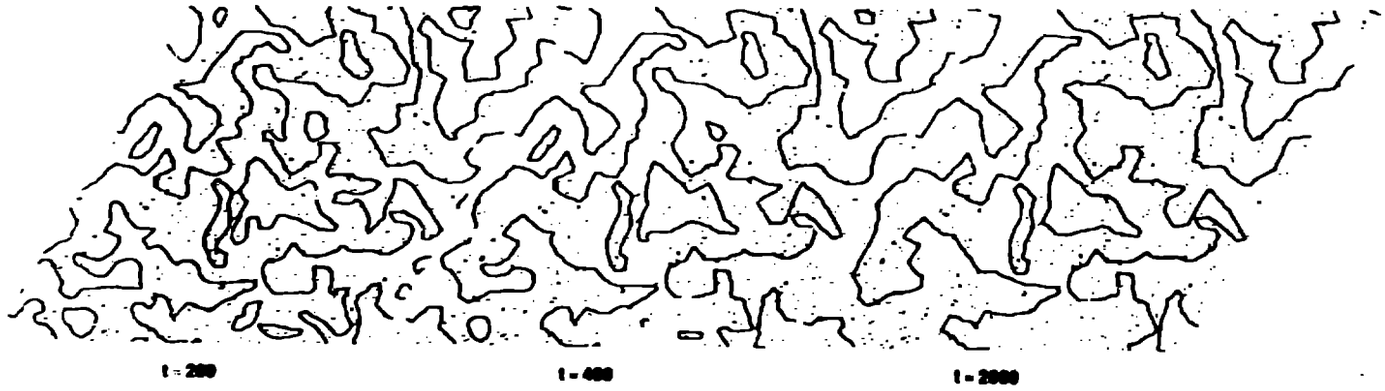

1. Evolution of the domain structure for the nonconserved Ising model quenched to T=0 on a 500x500 triangular lattice with c=0.005.

4. Evolution of the domain structure for the nonconserved Ising model quenched to T=1.3J/k_B on a 500x500 triangular lattice with c=0.01.

6. Evolution of the domain structure for the nonconserved Q=12 Potts model quenched to T=0 on a 200x200 triangular lattice with c=0.01.

account for impurities, the normal Potts model is modified to allow $0 \le S_i \le Q$, where $S_i=0$ corresponds to an impurity site [5,6].

The model was initialized by randomly placing Nc impurities with $S_i=0$ on the lattice, where N is the number of lattice sites and c is the concentration of quenched-impurities. The remaining sites were assigned a random value between 1 and Q. During the course of the quenched impurity simulations the impurity sites were not updated and hence both the impurity positions and concentration were time independent. The surface (line) energy of an impurity interacting with a spin on a NN site is the same as the domain-boundary energy between two sites with $S_i \neq S_j \neq 0$. The static impurity simulations were performed on a 200x200 triangular lattice for Q>4, on a 400x400 triangular lattice for Q = 3 or 4, and on a 500x500 triangular lattice for Q=2 (i.e., the Ising model). For Q<48, results of ten configurations were averaged for each value of Q and c. For Q=48, five simulations were performed for $c \ge 0.02$ and two for smaller values of c.

The diffusing-impurity simulations [7] were all performed on the Ising model on the square lattice. It is convenient to write the Ising Hamiltonian as

$$H = -J \sum S_i S_j \qquad (2)$$

where the spins are now $S_i = \pm 1$. As before, impurities correspond to $S_i=0$. The nonzero spins were updated using spin-flip dynamics. The impurity spins, on the other hand, were updated using spin-exchange (Kawasaki) dynamics, since the concentration of impurity sites is conserved. The same spin-updating probability (W) was employed for both impurity and non-impurity spins, i.e.

$$W = (D/2)[1+\tanh(-\Delta E/k_B T)] \qquad (3)$$

where ΔE is the difference in the energy of the system following and prior to a spin update and $k_B T$ is the thermal energy. The parameter D was chosen as unity for the non-impurity spins, and was assigned a value less than or equal to 1 for the impurity spins. Since D determines how often impurity and non-impurity site exchanges are attempted, D is proportional to the impurity diffusivity. The diffusing-impurity simulations were performed on 250x250 square lattices at $T=0.08J/k_B$. Simulations were performed for $0 \le D \le 1$ and $0.003 \le c \le 0.1$. Due to the large number of simulations required to examine this two-dimensional parameter space, only two simulations were performed for each set of conditions.

Several different methods are available for characterizing the degree of order in the system as a function of time. We have found [7] that the mean chord length, L, the inverse perimeter density, R_1, and the inverse square root of the second moment of the structure factor, $2\pi k_2^{-1/2}$, all yield approximately the same domain-growth exponent. However, the inverse perimeter density <R> was the most efficient to calculate and, hence, will be employed here. Noting that, at low temperature, the perimeter density is inversely proportional to the excess energy (over the ground-state energy E_o), we write

$$\langle R \rangle = -E_o/[E(t)-E_o] \qquad (4)$$

where E(t) is the energy of the system at time t. Since the ground-state energy of the non-impurity spins is a function of the instantaneous impurity configuration, the time dependence of E_o must be carefully accounted for.

1. Static Impurities

A. The Ising Model

In Fig. 1, we show the evolution of the spin configuration for the nonconservative Ising model quenched from $T=\infty$ to T=0 with c=0.005. While domain growth is evident between 200 and 400 Monte Carlo Steps (MCS), little domain

growth occurs between 400 and 2000 MCS. The pinned configuration (at 2000 MCS) shows fairly irregular domain walls. Fig. 2 shows the evolution of the domain size with time for five different impurity concentrations. At early times, all of the curves fall on the same line, corresponding to $\langle R \rangle \sim t^{1/2}$. At later times, however, the curves corresponding to nonzero c flatten out, indicating that the structure becomes pinned. The final domain size R_f is seen to increase with decreasing impurity concentration. A double logarithmic plot of R_f versus 1/c (Fig. 3) shows that the final, pinned domain size is inversely proportional to the square root of the impurity concentration. Such scaling relations collapse all of the data [5] onto a single curve obtained by plotting $\ln(R(t)/t^{1/2})$ versus $\ln(ct)$.

The microstructural evolution corresponding to a quench to $T \sim 0.7T_c$ with c=0.01 is shown in Fig. 4. Unlike for the quenches to T=0, the domain walls in this case are relatively smooth and considerable evolution of the structure is apparent between 400 and 800 MCS. The evolution of the domain size, $\langle R \rangle$, with time is shown in Fig. 5 for c=0.1 and quenches to T=0, 0.25J, 0.45J, 0.9J, and 1.3J. As for the quenches to T=0, all of the curves collapse at early times. While the curves do separate at later times, a well-defined, pinned configuration ($\langle R \rangle$ = constant) does not occur, indicating thermal activation over the impurity pinning sites. This activated depinning clearly becomes increasingly effective with increasing temperature. Attempts to calculate a growth exponent based on the curves in Fig. 5 yield exponents which vary with time: in other words, the system is not executing power-law growth. The exponents measured at the latest times in the figure increase with increasing temperature (from zero at T=0 to nearly 1/2 at T=1.3J), again supporting the notion of thermally activated domain growth.

B. The Potts Model

In addition to the Q=2 (Ising) limit discussed above, the effects of impurities on domain growth in the Potts model were examined for Q = 3, 6, 12, 24, and 48 [6]. Figure 6 shows the evolution of the microstructure for a quench to T=0 with c=0.01. Unlike in the Ising model, where domain walls never cross, for $Q \geq 3$ (in two dimensions), the domain walls meet at three-fold vertices. This results in relatively compact domains. The temporal evolution of the mean domain area ($A \sim R^2$) is shown in Fig. 7 for c=0.01 with Q = 3, 6, 12, and 24. Figure 8 presents similar data, but for fixed Q (=4) and varying c. All of these curves show a slope of order 0.5 at early times and become flat at late times, indicating pinning. Pinning occurs at smaller domain sizes with increasing Q and c. Plots of the final, pinned domain size (area) versus the inverse impurity concentration (Fig. 9) are all linear, with a slope that is Q dependent. An excellent fit to all of this data is provided by the following empirical functional form:

$$A_f = (1/c)\ [3+B/(Q-1)^{3/2}] \qquad (5)$$

where B is a constant.

4. Diffusing Impurities

When the impurities are free to diffuse [7], three new effects can occur: 1) the impurities can diffuse to domain walls, 2) the impurities can diffuse along with moving domain walls, and 3) the impurities can cluster. All of these features can be seen by comparing Figs. 10 and 11, which show the temporal evolution of an Ising model on a square lattice quenched from T=∞ to T=0 with c=0.01 and with D = 0 or 1, respectively. The most notable effect is that, when the impurity diffusivity is finite, the final or pinned domain size is smaller than when the impurities are static (D=0). Additionally, in the pinned configuration of the D=0 simulation relatively few impurities are observed in the center of the domains (i.e., away from domain walls). The effect of variations of D (diffusivity), at fixed c, on the rate of domain growth is indicated in Fig. 12. This figure clearly shows that increasing diffusivity leads to earlier pinning at

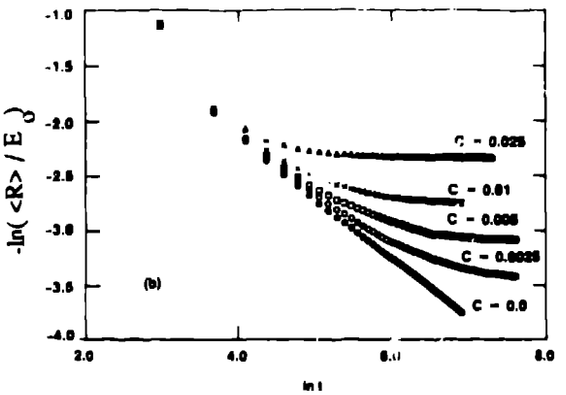

2. Normalized domain size vs time for the Ising model quenched to T=0. The data are averaged over 10 runs on a 500x500 lattice.

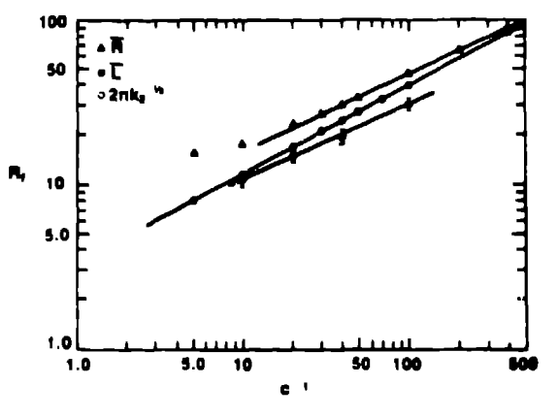

3. Log-log plot of the pinned domain size, R_f, vs the inverse concentration, c^{-1}. The three different measures are defined in the text.

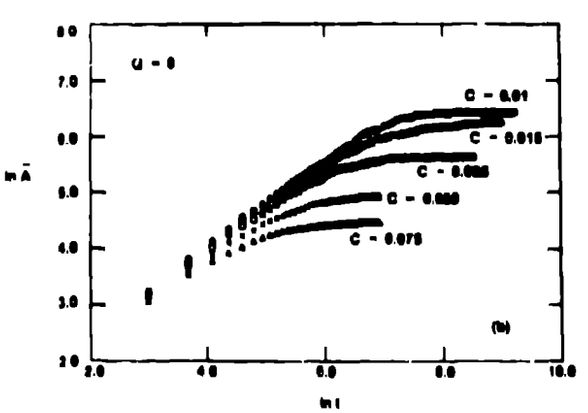

8. The average domain area vs time for T=0 quenches of the Q = 6 Potts model with c = 0.01, 0.015, 0.025, 0.050, and 0.075.

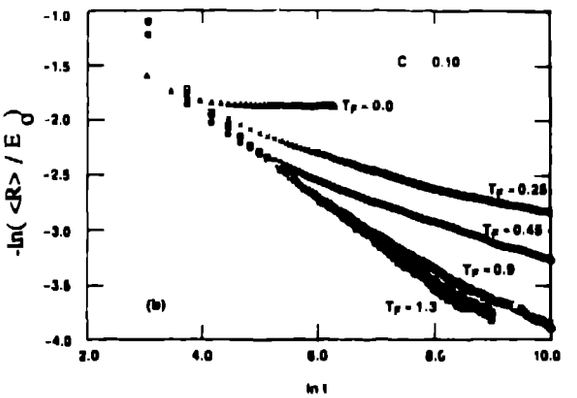

5. Normalized domain size vs time for the Ising model quenched to different temperatures for c=0.10.

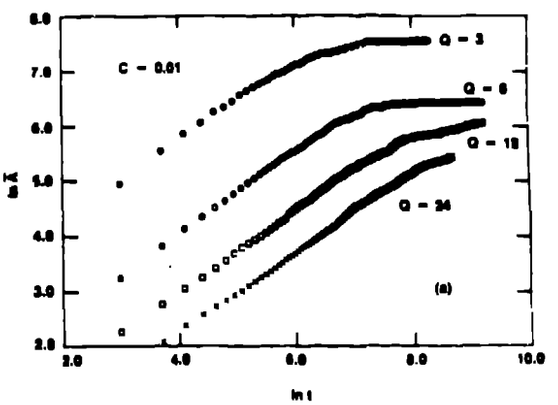

7. The average domain area vs time for T=0 quenches of the Q = 3, 6, 12, and 24 Potts model with c = 0.01.

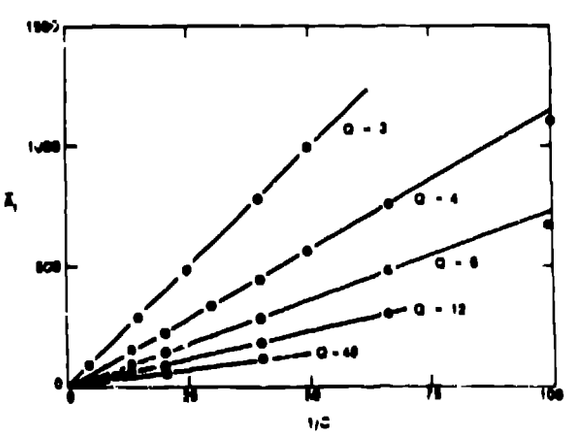

9. The pinned domain area, A_f, vs the inverse impurity concentration, 1/c, for Q = 3, 4, 6, 12, and 48.

smaller domain sizes. Similar results were obtained for all nonzero impurity concentrations simulated.

A great deal can be learned by examining the time dependence of the density of impurities on domain walls (see Fig. 13). While the fraction of impurities on domain walls generally show a decrease with time, the density of impurities along the domain walls (i.e., the number of impurities per unit domain wall length) increases with time, since $\langle R \rangle \sim t^{1/2}$, at least at early times. These curves appear to show a break that occurs at later times with decreasing D. This is most clearly seen in the D=0.3 curve, where the edge fraction initially decreases with time and then increases. At early times, the domains are small and the domain-wall curvature is large, and, hence, the domain-wall velocity is large. When the domain wall velocity is large, the impurities are not able to diffuse at a sufficiently high velocity to keep up with the domain wall. However, at later times, the domain size has grown, the domain-wall curvature and velocity have decreased, and, hence, the impurities can diffuse at rates sufficient to allow the domain walls to sweep impurities. The slower the domain wall, the more impurities it collects, and, as a result, it moves even slower. This feedback mechanism results in the catastrophic pinning of domain walls.

5. Analytic Results

To provide some theoretical insight into the above data, we [8] have performed an analytical analysis of the interaction between moving domain walls and diffusing impurities for a realistic form of the impurity--domain-wall interaction energy. This interaction energy is derived within the framework of the modified sine-Gordon model with either misfit impurities (coupling to the gradient of the order parameter) or elastic-modulus impurities (coupling directly to the order parameter). This interaction potential is then employed in calculating the steady-state impurity-concentration profile about a moving domain wall for arbitrary domain wall velocity and impurity diffusivity. At low velocities, the concentration profile is nearly symmetric about the position of the domain wall. As the velocity increases, the amplitude of the concentration profile decreases and the profile becomes increasingly asymmetric. The drag on the wall exerted by the impurities is given by

$$F_{drag} = \int_{-\infty}^{\infty} c(u) \, [-dE(u)/du] \, du \qquad (6)$$

where c(u) is the steady-state impurity concentration, E is the impurity--domain-wall interaction energy, and u is the separation of the impurity from the domain wall.

Eq. (6) can be evaluated analytically and then inverted to yield the steady state relation between the applied force on a domain wall and its resultant velocity. In the high-diffusivity/weak-interaction limit, this reduces to a linear force-velocity relation at small driving forces, an inflection at larger forces followed by another linear region, and, finally, saturation to an asymptotic velocity corresponding to the speed of sound in the material (Fig. 14a). The inflection in the curve is due to a transition from impurity-limited domain-wall motion to a regime in which the diffusing impurities are essentially incapable of keeping up with the domain wall. For strong-impurity--domain-wall interactions and lower impurity diffusivity, this inflection turns into a bifurcation with both high- and low-velocity branches (Fig. 14b). As the domain wall is quasi-statically accelerated from rest, it moves along the low-velocity branch until a critical force is applied, after which the domain wall travels at a velocity determined by the upper branch. Similarly, when the domain wall is slowed from high velocity it traverses the upper branch and then discontinuously moves to the lower one at a lower critical applied force. Relatively simple

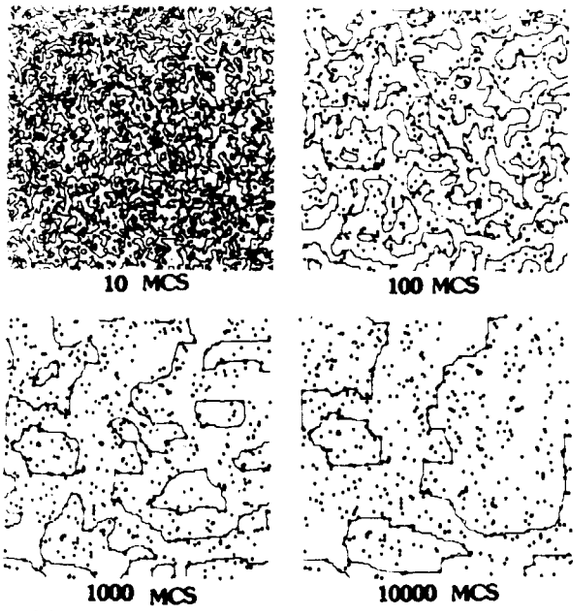

10. Evolution of the domain structure for the nonconserved Ising model quenched to $T=0.04J/k_B$ on a 200x200 triangular lattice with c=0.01 and D=0.

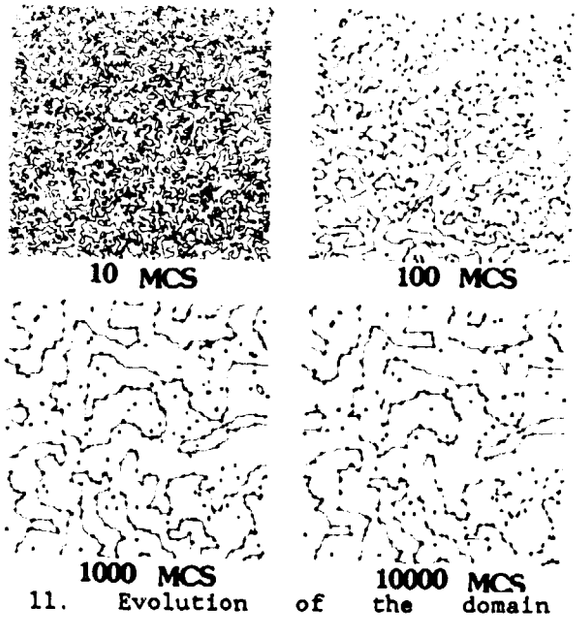

11. Evolution of the domain structure for the nonconserved Ising model quenched to $T=0.04J/k_B$ on a 200x200 triangular lattice with c=0.01 and D=1.

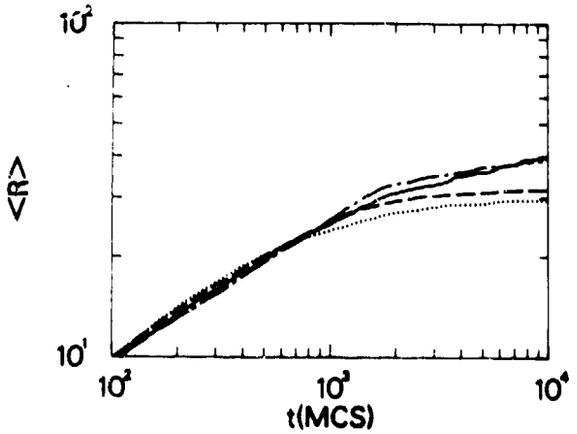

12. The mean domain size vs time for the Ising model with c=0.01. The dotted, dashed, chain-dotted, and solid curves correspond to D=1,0.3,0.1,0.03,0, respectively.

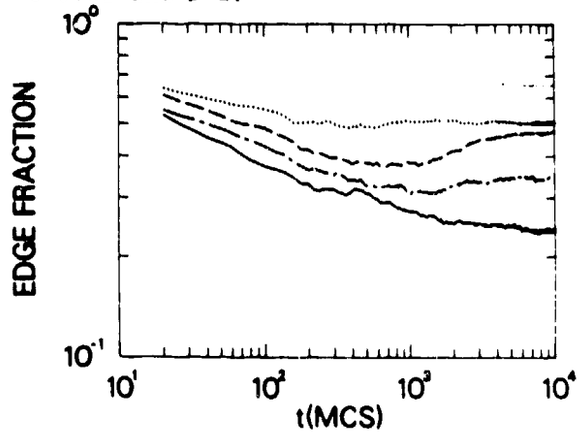

13. The fraction of impurities on domain edges (boundaries) as a function of time for c=0.01. The curves correspond to the impurity diffusivities considered in Fig. 12.

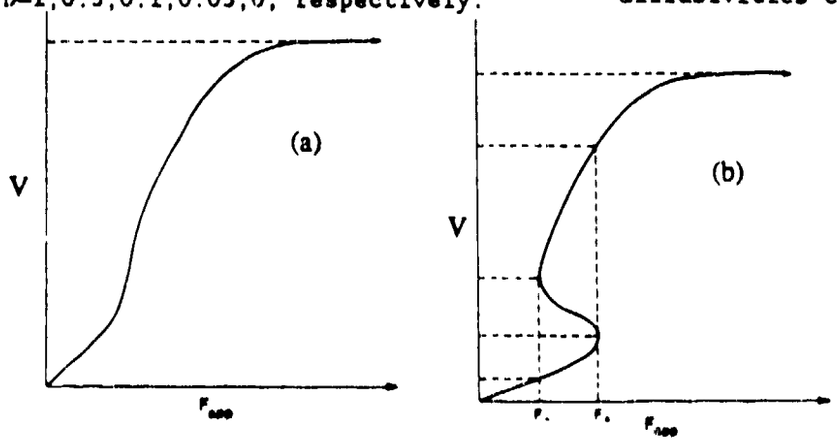

14. Qualitative forms of the domain-wall velocity vs applied force. The transition from impurity-dominated behavior to impurity-free behavior can be either (a) gradual or (b) hysteretic.

expressions for the critical points on the hysteresis loop have been obtained in different limits.

Application of these results to domain growth in the presence of impurities confirms the qualitative picture described above (at the end of Section 4). Following the quench to low temperature, the domain-wall velocity is initially high due to the large-curvature driving force at small domain size and then slows as the domain size increases (decreasing driving force). If conditions are such that the force-velocity relation depicted in Fig. 1*b is applicable, the domain-wall velocity will decrease slowly during domain growth until its velocity falls below a critical value where it is captured by the impurities and slowed very drastically, if not effectively pinned. Since different domain walls will be moving with different velocities during domain growth, the pinning of the system is expected to occur one domain wall at a time until no walls are free. If the temperature is such that significant domain-wall velocities are possible in the regime where the impurities are diffusing along with the walls (i.e., the lower branch), then further domain growth can occur, although with an effectively enhanced damping. It is interesting to note that, once the system finds itself in the regime where the impurities can keep up with the domain walls, the effective bulk concentration of impurities is reduced (i.e., a non-negligible fraction of the impurities is on the walls), and a moving wall feels a smaller impurity drag than expected based on the total impurity concentration. It is expected that this will lead to a rescaling of the steady state.

6. Conclusions

Recent Monte Carlo simulations on the effects of impurities on domain growth [5-7] show that, at low temperatures, there is a rather abrupt transition from normal domain growth (i.e., $R \sim t^{1/2}$) to a pinned state. The mean, pinned domain size decreases with increasing degeneracy and with increasing impurity concentration as $R_f \sim c^{-1/2}$. This transition is less abrupt and, with increasing temperature, it occurs at larger domain size and later times. When the impurities are free to diffuse, they slow domain growth by diffusing to and diffusing along with moving domain walls. Increasing diffusivity results in decreased final domain sizes, at least at low temperatures. A one-dimensional analytical analysis [8] shows that the presence of diffusing impurities can lead to nonlinearities and hysteresis in the relationship between the driving force on a domain wall and the resultant domain-wall velocity and, hence, non-classical domain growth exponents.

References

1. M. P. Anderson, D. J. Srolovitz, G. S. Grest, and P. S. Sahni: Acta Metall. 32, 783 (1984).
2. D. J. Srolovitz, M. P. Anderson, P. S. Sahni, and G. S. Grest: Acta Metall. 32, 793 (1984).
3. J. L. Lebowitz, J. Marro, and M. H. Kalos: Acta Metall. 30, 297 (1982).
4. F. Haessner: Recrystallization of Metallic Materials, (Riederer Verlag, Berlin 1978).
5. G. S. Grest and D. J. Srolovitz: Phys. Rev. B 32, 3014 (1985).
6. D. J. Srolovitz and G. S. Grest: Phys. Rev. B 32, 3021 (1985).
7. D. J. Srolovitz and G. N. Hassold: Phys. Rev. B 35, 6902 (1987).
8. D. J. Srolovitz, R. Eykholt, D. M. Barnett, and J. P. Hirth: Phys. Rev. B 35, 6107 (1987).
9. A. B. Bortz, M. H. Kalos, and J. L. Lebowitz: J. Comput. Phys. 17, 10 (1975).